Journal of Statistical Physics, Vol. 112, Nos. 5/6, September 2003 (© 2003)

Dynamic Transition in a Binary Liquid and Its Dependence on the Mass-Ratio: Results from a Self Consistent Mode Coupling Model

Upendra Harbola[1] **and Shankar P. Das**[1]

Received October 4, 2002; accepted March 18, 2003

We use the self-consistent mode coupling model for binary mixtures to investigate the influence of the mass-ratio (m_2/m_1) of constituent particles, where subscripts 1 and 2, respectively, denote the smaller and bigger size particles, on the dynamic transition. For the higher values of the ratio, $m_2/m_1 \geqslant 2$, we find that there is no significant change in the transition point. This is in qualitative agreement with the simulation studies on the binary mixtures. However, for the case of bigger particle mass, m_2, being much smaller than that of the smaller particle mass, m_1, a significant change in the transition point is observed. The dependence of the non-ergodicity parameters on the mass-ratio is also predicted for different wave numbers. We also estimate the range in the vicinity of the dynamic transition point where the square root cusp behavior of the non-ergodicity parameter (NEP) dominates.

KEY WORDS: Fluctuating hydrodynamics; binary mixture; mode-coupling.

1. INTRODUCTION

The self consistent Mode-Coupling Theory (MCT)[1,2] is a useful tool for understanding the slow structural relaxation in the supercooled liquids. In the simple form the theory predicts a sharp transition of the supercooled liquid from ergodic to non-ergodic phase. This so called "ideal" glass transition occurs at a critical density (n_c) at which the time scales associated with the structural relaxation diverge. The long time limit of density correlator, known as the nonergodicity parameter (NEP), $f(q)$, is treated as an order parameter for the transition. A nonzero value for $f(q)$ signifies the nonergodic state of the system. Subsequently[3] it was demonstrated

[1] School of Physical Sciences, Jawaharlal Nehru University, New Delhi 110067, India; e-mail: shankar0359@yahoo.com and sdas0700@mail.jnu.ac.in

0022-4715/03/0900-1109/0 © 2003 Plenum Publishing Corporation

that in a compressible fluid, the sharp transition is smeared by the inclusion of the coupling of current correlation with density fluctuations. This leads to the ergodicity on a sufficiently long time scale even for $n > n_c$. However this sharp transition predicted in the simple form of the MCT strongly effects the dynamics of supercooled liquid and has been investigated widely through theoretical[4] and other techniques.[5] In the immediate vicinity of the transition point, the NEP follows a cusp behavior,[6, 7]

$$f(q) = f^c(q) + A_o h(q)\, \epsilon^{1/2} + O(\epsilon), \tag{1}$$

where superscript c indicates the NEP at the critical point of transition and A_o is a positive constant factor. $\epsilon = \eta/\eta_c - 1$ is the parameter which represents the relative distance from the transition point where η_c is the total packing fraction (η) at the transition point. $h(q)$ is the wavevector dependent scaling amplitude calculated at the critical point. Usually the binary system is described by three independent parameters: (a) The fractional concentration of bigger particles $x = n_2/(n_1 + n_2)$; (b) The size ratio α $(= \sigma_1/\sigma_2)$, of the diameters of the two species; and (c) The total packing fraction $\eta = \eta_1 + \eta_2$ where η_1 and η_2 are the packing fractions of the individual species, i.e., $\eta_s = \pi n_s \sigma_s^3/6$, n_s being the number of particles per unit volume of sth species. We take σ_2, diameter of bigger species, as the unit of length. A relatively less studied parameter is the mass-ratio, $\Re = m_2/m_1$, of the particles of the two species. In earlier MCT models for the Glass transition in a binary liquid the theoretical predictions do not depend on this ratio.[8] The model studied in ref. 9, on the other hand, shows that the dynamic transition predicted by the model is related to the mass-ratio of the two species. The results from the theoretical model as obtained here are in qualitative agreement with the molecular dynamics (MD) simulations.[10, 11] We also study the range of validity of the square root cusp behavior of the NEPs approaching the dynamic transition point from the nonergodic state.

In the next section, we present a brief review of the MCT model for binary systems and obtain the q dependent scaling amplitudes. In Section 3, we present our results on hard sphere as well as Lennard-Jones systems. We conclude the present work with a short discussion of our results in Section 4.

2. MODEL FOR THE DYNAMICS OF A TWO COMPONENT FLUID

2.1. Nonlinear Fluctuating Hydrodynamics

We give an overview of the MCT for the binary mixtures. A detail discussion of the model can be found in ref. 9. In a binary mixture the

slow hydrodynamic modes correspond to the set of conserved variables in the system. These conserved variables are the two partial densities ρ_s, $(s=1, 2)$, total momentum density $\vec{g}$ and the energy density. Using the standard methods,[12] the time evolution of fluctuations of conserved variables is described by the dynamical equations,

$$\frac{\partial \rho_s}{\partial t} + \nabla \cdot \left[\frac{\rho_s}{\rho} \vec{g} \right] + \gamma_{ss'} \frac{\delta F_u}{\delta \rho_{s'}} = \theta_s, \qquad s = 1, 2 \tag{2}$$

$$\frac{\partial g_i}{\partial t} + \nabla_j \frac{g_i g_j}{\rho} + \rho_s \nabla_i \frac{\delta F_u}{\delta \rho_s} + L_{ij} \frac{\delta F}{\delta g_j} = f_i, \tag{3}$$

where the repeated indices are summed over—we will use this convention throughout the paper. θ_s and f_i, respectively, represent the noises that correspond to the fluctuations in partial density of sth species and the ith component of the total momentum density. Total free energy $F = F_k + F_u$. F_k and F_u, respectively, represent the kinetic and interaction parts given by,

$$F_k = \frac{1}{2} \int dx \frac{g^2(x)}{\rho(x)} \tag{4}$$

$$F_u = \frac{1}{m_s} \int dx\, \rho_s(x) \left[\ln \frac{\rho_s}{\rho_{0s}} - 1 \right] - \frac{1}{2m_s m_{s'}} \int dx\, dx'\, c_{ss'}(x-x')\, \delta\rho_s(x)\, \delta\rho_{s'}(x'), \tag{5}$$

where m_s and ρ_{0s} represent the mass and average mass-density of the sth species. $c_{ss'}(x)$ is the direct correlation function between s and s'. $\delta\rho_s(x) = \rho_s(x, t) - \rho_{0s}$ is the fluctuation in the density of the sth species. The bare transport coefficients L_{ij} and $\gamma_{ss'}$, respectively, refer to the viscous dissipation and the particle interdiffusion in the system and are related to the corresponding noises through the fluctuation dissipation relations. Since total density $\rho = \rho_1 + \rho_2$ satisfies the continuity relation, the noises corresponding to the two density variables must satisfy $\theta_1 + \theta_2 = 0$ and here we have assumed[13] $\gamma_{ss'}(x) = \nabla^2 \gamma_0(x)(-1)^{s+s'}$. For an isotropic system, L_{ij} can be splitted into the longitudinal and transverse parts as, $L_{ij}(q) = q_i q_j \Gamma_0 + (q^2 \delta_{ij} - q_i q_j)\, \zeta_0$, where $L_{ij}(q)$ is the Fourier transform of $L_{ij}(x)$. Γ_0 and ζ_0, respectively, represent the bare longitudinal and transverse[13] viscosities in the system.

2.2. Dynamical Equations for the Correlation Functions

The mode-coupling equations for the binary mixture deal with the 2×2 matrix of the correlations of the density fluctuations defined as,

$$C_{ss'}(q, t) = \frac{1}{N} \langle \delta\rho_s(q, t)\, \delta\rho_{s'}(-q, 0) \rangle, \tag{6}$$

where N represents the total number of particles in the system. From Eqs. (2)–(5), we obtain a matrix equation,

$$[z\mathrm{I} - M(q, z)]\, C(q, z) = \chi(q), \tag{7}$$

for the partial density correlation function matrix $C(q, z)$. Here $C(q, z)$ is the Laplace transform of the partial density correlation matrix $C(q, t)$ and I represents the identity matrix. $\chi_{ss'} = a_s a_{s'} S_{ss'}$ is the equal-time density correlation function matrix. $a_s = m_s \sqrt{n_s}$ and $S_{ss'}$ is the partial structure factor between s and s'. The matrix $M(q, z)$ in Eq. (7) is given by,

$$M(q, z) = q^2 [\imath v(q) + \{z + \imath q^2 \Gamma^{\mathrm{R}}(q, z)\}^{-1}\, \tilde{\Delta}]\, \chi^{-1}(q), \tag{8}$$

where matrices $v_{ss'}(q) = \gamma_0(q)(-1)^{s+s'}$ and $\tilde{\Delta}_{ss'} = \rho_0 x_s x_{s'}$, with $x_s = \rho_{0s}/\rho_0$. The renormalized longitudinal viscosity, Γ^{R}, has two parts,

$$\Gamma^{\mathrm{R}} = \Gamma_0 + \Gamma^{\mathrm{mc}}, \tag{9}$$

where Γ^{mc} represents the mode-coupling contribution. Up to the one loop order, the MC contribution is given by,

$$\Gamma^{\mathrm{mc}}(q, t) = \frac{\Omega_q}{2q^2} \int \frac{dk}{(2\pi)^3} V_{ss'}(q, k)\, V_{ll'}(q, k_1)\, C_{l's'}(q, t)\, C_{ls}(k_1, t), \tag{10}$$

where $k_1 = q - k$ and the vertex function is given by,

$$V_{ss'}(q, k) = (a_s a_{s'})^{-1}\, [\hat{q}.k\ \tilde{c}_{ss'}(k) + \hat{q}.k_1\ \tilde{c}_{ss'}(k_1)]. \tag{11}$$

The quantity $\Omega_q = \sum_{ss'} \Delta_{ss'} S_{ss'}(q)$ where $\Delta_{11} = n_1 A^{-1}$, $\Delta_{22} = \Re^2 n_2 A^{-1}$, and $\Delta_{12} = \Delta_{21} = \Re^2 \sqrt{n_1 n_2}\, A^{-1}$ with $A = (n_1 + \Re^2 n_2)$.

2.3. The Dynamic Transition to Nonergodic Phase

The long-time limit of the normalized density correlation functions defined as, $f_{ss'}(q) = C_{ss'}(q, t \to \infty)/\sqrt{\chi_{ss}\chi_{s's'}}$, is termed as the non-ergodicity

parameter (NEP). From Eq. (7) one obtains, in the asymptotic limit of long times, the following set of self-consistent equations for NEPs,[9]

$$f_{ss'}(q) = \Im_{ss'}(q)\left[\frac{\Gamma_q}{1+\Gamma_q}\right], \tag{12}$$

where Γ_q is the long time limit of the MC kernel given in Eq. (10). $\Im(q)$ is the structure dependent quantity,

$$\Im_{ss'}(q) = \frac{\Delta_{ij} S_{is}(q)\, S_{js'}(q)}{\Omega_q [S_{ss}(q)\, S_{s's'}(q)]^{\frac{1}{2}}}. \tag{13}$$

Equation (12) constitute a set of coupled nonlinear integral equations for the non-ergodicity parameters $f_{ss'}$. The dynamic instability of the ideal glass transition in the binary system is then located from the *self-consistent* solution of Eq. (12) by iterative method in a similar manner as is done for the one-component systems.

In the following expressions, we will represent the double index $\{ss'\}$ with a single index (a or b). With this notation, the variation in the NEP, f_a^q, in the vicinity of the transition point can be written as,

$$f_a(q) = f_a^c(q) + \kappa_a(q)\, g_a(q), \tag{14}$$

where $\kappa_a(q)$ is defined as,

$$\kappa_a(q) = \left[1 - \frac{f_a^C(q)}{\Im_a^q}\right]^2. \tag{15}$$

$\kappa_a(q)$ is a set of 4R numbers, R being the number of grid points in the wavevector q. $g_a(q) \to 0$ as the transition point is approached $\epsilon \to 0$. Making a Taylor expansion of $f_a(q)$ around the ideal transition point and using Eqs. (12) and (14), we obtain a matrix equation,

$$g_a(q) = \sum_{k,\,b} C_{ab}^{(1)}(qk)\, g_b(k) + \sum_{bc,\,kp} C_{abc}^{(2)}(qkp)\, g_b(k)\, g_c(p) + \epsilon C_\eta^q + O(\epsilon^2, g^2), \tag{16}$$

where the matrices $C^{(1)}$, $C^{(2)}$ are given by,

$$C_{ab}^{(1)}(qk) = \left[\Im_a^q \frac{\delta \Gamma_q}{\delta f_b(k)}\right] \kappa_b(k) \tag{17}$$

$$C_{abc}^{(2)}(qkp) = \left[\Im_a^q \left\{\frac{1}{2}\frac{\delta^2 \Gamma_q}{\delta f_b(k)\, \delta f_c(p)} - \frac{1}{1+\Gamma_q}\frac{\delta \Gamma_q}{\delta f_b(k)}\frac{\delta \Gamma_q}{\delta f_c(p)}\right\}\right] \kappa_b(k)\, \kappa_c(p). \tag{18}$$

Here quantities within the square brackets in Eqs. (17) and (18) are evaluated at the critical point and,

$$C_{\eta}^{q} = \eta \frac{\delta \Gamma_q}{\delta \eta}. \tag{19}$$

Now a solution of Eq. (12) at the critical point involves solving Eq. (16) for $\eta = \eta_c$. Using the expansion $g_a(q) = \epsilon^{\frac{1}{2}} g_a^{(1)}(q) + \epsilon g_a^{(2)}(q) + O(\epsilon^2)$ in Eq. (16) and collecting the terms of leading order in ϵ, we obtain the equation,

$$g_a^{(1)} = C_{ab}^{(1)}(qk)\, g_b^{(1)}(k). \tag{20}$$

Since in the present work we are interested only in the leading order solution of Eq. (16), we will drop the superscript 1 from the following expressions. Equation (20) is then put in to an eigenvalue problem in terms of the stability matrix, C, as defined in Eq. (17). This is a $4\mathrm{R} \times 4\mathrm{R}$ matrix and the eigenvector $g_b(k)$ has 4R elements. The numerical solution of Eqs. (20) shows that the maximum eigenvalue λ_0 of the stability matrix is non-degenerate and $0 < \lambda_0 \leqslant 1$. As the transition is approached, $\lambda_0 \to 1$. The normalized left and right eigenvectors of the stability matrix corresponding to the eigenvalue λ_0 are, respectively, denoted by $\hat{e}^q$ and e^q, and the normalization constants are determined by the conditions,

$$\sum_{q,\,a} (1+\Gamma_q)^{-1}\, \hat{e}_a(q)\, \Im_a(q)\, e_a(q) = 1 \qquad \sum_{q} \hat{e}_a(q)\, e_a(q) = 1. \tag{21}$$

In the close vicinity of the transition point, the leading order term $O(\epsilon^{\frac{1}{2}})$ in Eq. (1) dominates over the higher order terms. Thus over the range where cusp behavior is dominant, the vector $h_a(q)$ is obtained as,

$$h_a(q) = \kappa_a(q)\, e_a(q). \tag{22}$$

This gives the q-dependence of the scaling amplitudes for the various NEPs near the transition point. We test the range of ϵ values where the leading order cusp behavior (1) matches with numerical solution of the integral Eq. (12).

3. RESULTS

3.1. Mass-Ratio and the Glass Transition

First we consider a hard sphere binary system characterized by the size ratio $\alpha(=\sigma_1/\sigma_2)$ of the two species and the relative composition x. Here $0 \leqslant \alpha \leqslant 1$ and $x = N_2/N$ denotes the relative concentration of the bigger

species in the mixture. In calculating the k-integral appearing in Eq. (10), the upper cut-off is chosen at $k^* = 40$. For a fixed value of $\Re = m_2/m_1$, where m_2 and m_1, respectively, denote the mass of bigger and smaller particles, the transition point depends upon the three independent parameters: size ratio α, total packing fraction, η and x. In order to locate the transition point for the HS system, we solve Eqs. (10) and (12) self-consistently using the Percus–Yevick (PY) structure factor[14, 15] as input. We find that if $\alpha \leqslant 0.8$ and $\Re = 1$, there is a range of x over which the dynamic transition does not occur up to fairly large η value.[9]

In order to study the $\Re$ dependence of the dynamic transition, we have chosen the two different sets of parameter values, namely $x = 0.7$, $\alpha = 0.8$, and $x = 0.5$, $\alpha = 0.83$. Here the latter set of parameter values are same as considered in the MD-simulation in ref. 10. We list our main findings below.

(i) For $\Re \geqslant 1$, which implies that the bigger sized particles have more mass than the smaller ones, no significant change in the transition point is observed. The critical packing fraction η_c for transition to the non-ergodic phase is almost independent of $\Re$ for the above mentioned range. This result is in agreement with the trend seen in MD simulation of the binary mixtures.[10, 11]

(ii) However, if the mass corresponding to bigger particles becomes lesser than that for the smaller particles, i.e., $\Re \leqslant 1$, a significant change in the transition point is seen. In Fig. 1, we show the variation of transition

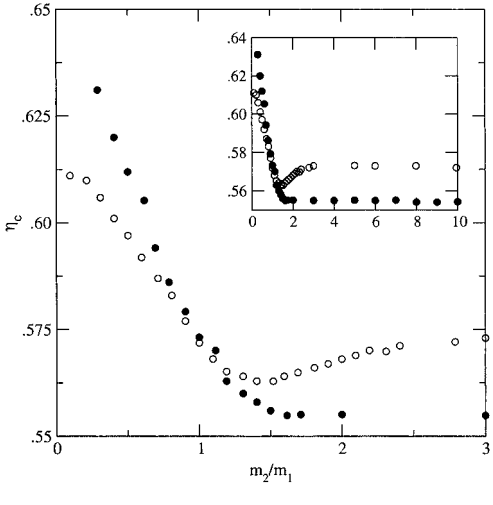

Fig. 1. Variation in the transition point with $\Re$ (see text) is shown for two set of parameter values $x = 0.7$, $\alpha = 0.8$ (filled circles), and $x = 0.5$, $\alpha = 0.83$ (open circles). Inset: same quantity is shown for larger values of $\Re$.

point with $\Re$ for two different sets of thermodynamic parameters x and α. Filled circles correspond to $x = 0.70$ and $\alpha = 0.80$ while open circles are for $x = 0.50$ and $\alpha = 0.83$. In the inset, we have included the higher range of $\Re$ over which the transition density is almost constant.

Thus we observe that upon changing the value of $\Re$, the dynamic transition remains unaffected as long as the bigger particles are heavier than the smaller ones. But the scenario gets completely changed if the smaller particles are made more heavier than the bigger ones. In that case the transition density shifts to higher packing fraction.

We calculated the NEPs at the transition point for five different values of $\Re$ at fixed $x = 0.7$ and $\alpha = 0.8$. This is shown in Fig. 2(a) for the smaller species over a range $0 \leqslant q \leqslant 20$. Here the three different curves correspond to $\Re = 0.5$ (solid), 0.8 (dash dot), and 1.0 (dashed). In the inset, we plot the same quantity for $\Re = 1.5$ (dash) and 10.0 (solid). Corresponding results for the bigger particles are shown in Fig. 2(b). We find that over the large q range the NEP for the smaller species shows an increasing trend as $\Re$ is decreased. Over the same q range an opposite behavior is seen in the bigger particle case. In the smaller q range, however, the two NEPs show similar behavior with $\Re$.

The behavior of the NEPs for the small and big particles described above can be given a physical interpretation. The wave number and the mass ratio dependence of the NEP is driven by the influence of the structure on the dynamics. As the mass ratio is increased the bigger spheres

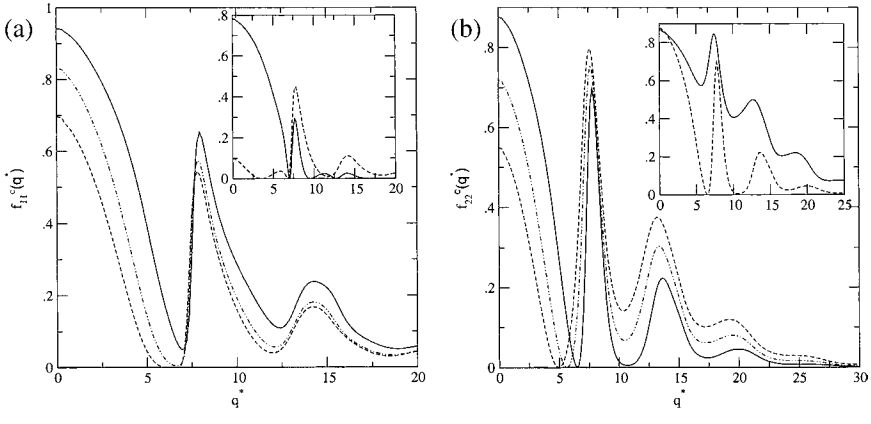

Fig. 2. (a) Critical NEPs corresponding to the smaller species, $f_{11}(q)$, are shown at three different values of $\Re = 0.5$ (solid), 0.8 (dash dot), and 1.0 (dashed), 0.8 (dash dotted), and 0.5 (dotted). Here parameter values $x = 0.7$, $\alpha = 0.8$. In the inset we show results for $\Re = 1.5$ (dash) and 10.0 (solid). (b) NEPs for the bigger particles are plotted at the same parameter values as in Fig. 2(b). Inset shows results for same $\Re$ values as in the inset of Fig. 2(b).

being heavier have a higher likelihood to get jammed and hence the extent of corresponding nonergodicity gets enhanced. The smaller spheres as a result get jammed in the cages formed by the frozen structure of bigger spheres. So over longer length scales, i.e., small q values, the tendency of the nonergodicity parameter for the smaller species is same (to increase with $\mathfrak{R}$) as that of the bigger spheres. However over shorter length scales the small (lighter) spheres move around relatively easily between the bigger spheres indicating a fall in the nonergodicity parameter for large q values. We also observe that this variation in the NEPs slows down as $\mathfrak{R}$ is increased and becomes almost independent of it for $\mathfrak{R} > 10$.

3.2. Scaling Analysis Near the Transition Point

Here we present our results on the scaling near the transition point. We also test the range of ϵ where the leading order cusp behavior of the NEP is dominant. We consider a mixture with $\alpha = 0.8$, $x = 0.7$, and $\mathfrak{R} = 1$. From the numerical solution of the matrix Eq. (20) together with the conditions (21), we obtain normalized eigen vectors $\hat{e}^q$ and e^q corresponding to the eigen value $\lambda_0 = 1$. The wavevector dependent scaling amplitudes $h_a(q)$ are then obtained from the matrix equation (22). The results are shown in Figs. 3(a) and 3(b) for the smaller and bigger particles, respectively. Inset shows results for the corresponding NEPs. From Fig. 3(a), we see that the amplitude h_q corresponding to the smaller particles go to very small values over some intermediate range of wavevector q lying between $6.0 \leqslant q \leqslant 7.0$. This is due to the structure dependent quantity $\mathfrak{I}(q)$ appearing in Eq. (12). The same behavior is seen in the NEP of the smaller particles and is shown in the inset of the figure. Similar behavior is found in case of bigger particles as shown in Fig. 3(b). However this intermediate q range over which NEPs fall to small values disappears as one moves toward the one component limit, i.e., $x \to 0$ or 1.[9] The results for the scaling amplitudes presented here reduce to the one-component results[7] under the appropriate limits.

In order to check the ϵ range over which the scaling (1) is valid, we calculate the quantity $\bar{f}_{ss'}(q) = \Delta f_{ss'}(q)/h_{ss'}(q)$, where $\Delta f_{ss'}(q) = f_{ss'}(q) - f^c_{ss'}(q)$, as a function of ϵ. Thus if the scaling proposed in Eq. (1) is valid, we expect all the points for different q values to fall on a single curve, $\bar{f}(q) = A\epsilon^{1/2}$, independent of the species. The results are shown in Fig. 4 for the q values around the bigger particle structure factor peak. The circles and triangles denote $\bar{f}(q)$ for the bigger and smaller particles, respectively. From the Fig. 4, we find that, indeed, all the points below $\epsilon = 0.001$ do fall on the curve $\bar{f}(q) = A\epsilon^{1/2}$, which is shown as a straight line with slope 0.5 and $A = 2.01$. This result shows that the cusp behavior predicted by the

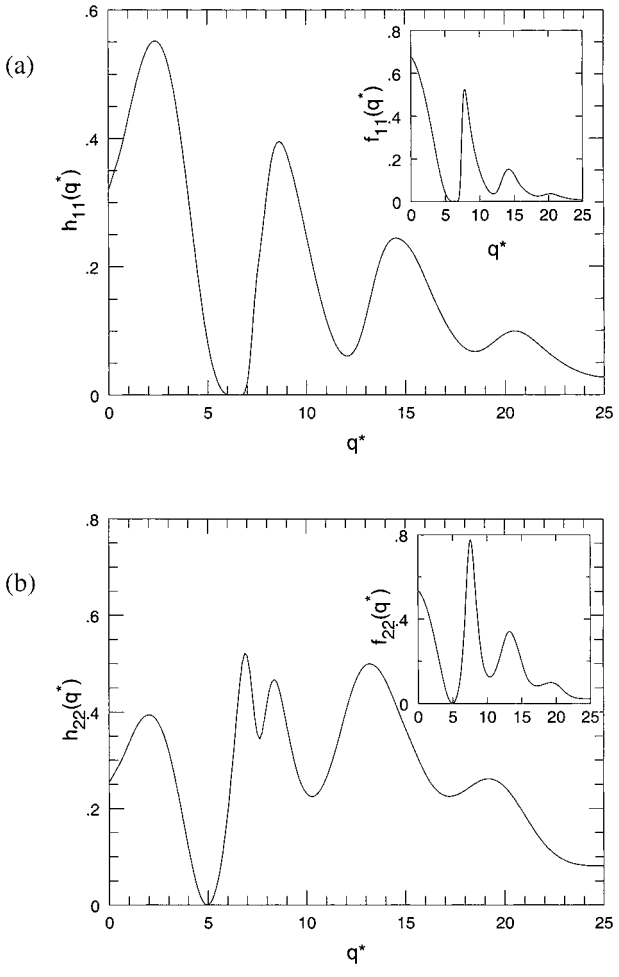

Fig. 3. (a) Wavevector dependent scaling amplitude is shown for smaller species $h_{11}(q)$ at $x = 0.7$, $\alpha = 0.8$, and $\eta = 0.574$ (transition density). Corresponding NEP is shown in the inset. (b) Wavevector dependent scaling amplitude for the bigger particles are shown at the same parameter values as in Fig. 3(a). Inset shows the corresponding NEP.

theory is observable only within 0.1% of the transition point. Using constant A, as obtained from Fig. 4, and the theoretical results for $h(q)$, we calculated $\Delta f_{ss'}(q)$ from Eq. (1). For comparison, we have shown both the theoretical (solid line) and numerical results (dots) for $\Delta f_{ss'}(q)$ in Figs. 5(a) and 5(b) for smaller and bigger particles, respectively. The two results match only for very small values of $\epsilon \leqslant 0.001$. Dotted lines in the figures show the results with the linear order term ($\sim O(\epsilon)$) included in Eq. (1).

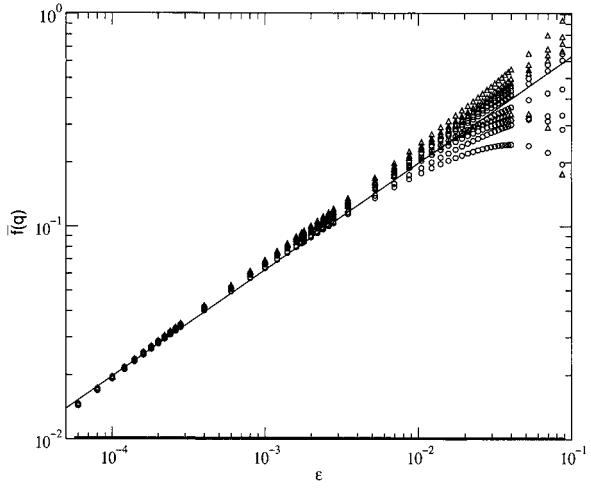

Fig. 4. Function $\bar{f}(q)$ (see text) is plotted as function of ϵ for different q values that lie around the first peak of the bigger particle structure factor. Triangles and circles denote the smaller and bigger particle results, respectively. Straight line represents the fit, $\bar{f}(q) = A\epsilon^{1/2}$ with $A = 2.01$.

This shows that beyond $\epsilon = 0.001$, the next higher order term starts dominating over the leading term of cusp behavior.

3.3. Absence of the Transition in LJ Potential

The model described above in Section 2 is also useful for studying glass transition in systems with other interaction potentials. Extensive simulation study has been done on the binary Lennard-Jones (LJ) system characterized by $x = 0.8$ and $\alpha = 0.88$ with mass-ratio unity.[16] For this system, a dynamic transition at temperature $T_c = 0.435$ was predicted from the simulation studies.[17] This critical temperature was obtained from a power law fit to the self-diffusion coefficient at low temperatures. In the present theoretical calculations with LJ system the simulation results for the static structure factors[16] as well as those from Integral equations[18] are used. From the self-consistent solution of Eqs. (10) and (12), we find that the model equations do not show any transition up to the lowest temperature $T = 0.466$ investigated in the simulation studies.[16] This aspect of the mode coupling models is new since the earlier models[19] when used with the *same* structure factors *show a dynamic transition at a much higher temperature* $T_c = 0.922$.[20] In order to study the lower temperatures, we used integral equation results[18] for the static structure factors. With these structure factors as an input, we solved the NEP equations (12) up to as

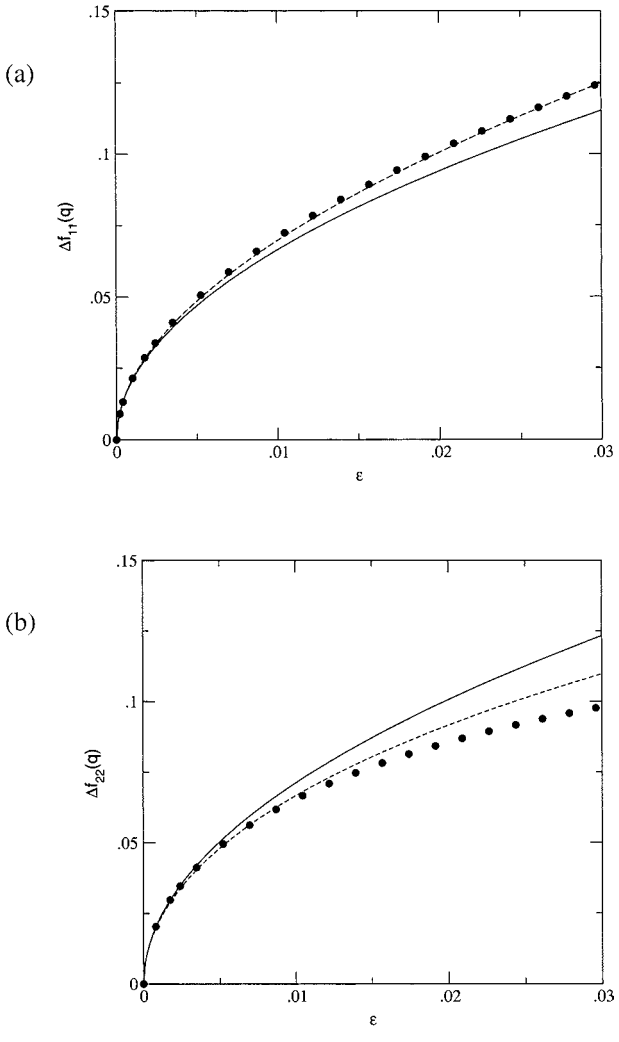

Fig. 5. (a) Function $\Delta f(q) = f(q) - f^c(q)$ is plotted for smaller species over a range of ϵ values at $q = 8.0$ (peak in smaller particle structure factor). Dots are the numerical results and solid line represents Eq. (1) with $A = 2.01$. Dotted line represents the fit with higher order term ($O(\epsilon)$) included in Eq. (1). (b) Same as in Fig. 5(a) but for bigger particles at $q = 7.80$.

low as $T = 0.3$ without any freezing in the system. On the other hand, for a some what similar HS system (with same x and α values) the transition occurs at $\eta_c = 0.534$. Since structure factor is the only input required in determining the transition point, we focus on the respective structures ($S(k)$) to look for a possible reason for this very different behaviors in the

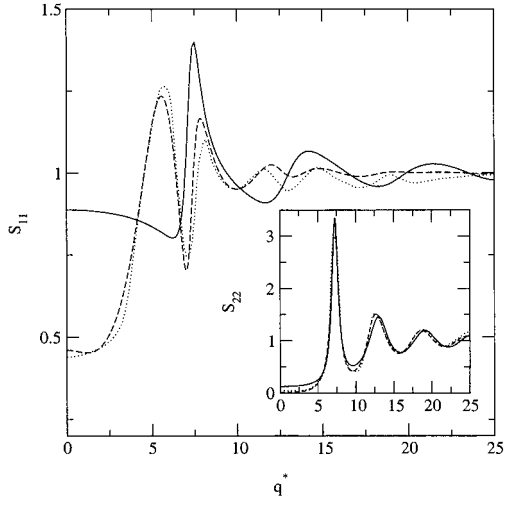

Fig. 6. Structure factors S_{11} and S_{22} (inset) for $x = 0.8$ and $\alpha = 0.88$: dotted and dashed curves, respectively, represent the simulation data of ref. 16 and the integral equation solution[18] for the LJ system at $T = 0.5$. Solid line is the Percus–Yevick results[14, 15] for the HS system at $\eta_c = 0.534$.

two systems. We find that bigger particle structure factors, S_{22}, for the two systems are very similar while the structure factors corresponding to the smaller particles, S_{11}, are quite different. In Fig. 6, we show the structure factors S_{11} for the HS system (solid line) at $\eta = 0.534$ and for LJ system of Kob–Andersen mixture at $T = 0.50$. We show both the simulation results (dotted) as well as that obtained from integral equations (dashed). The inset shows the corresponding results for S_{22}. Thus it is the structure of the smaller species which prevents the freezing of the LJ system at the lowest temperature investigated.

The present work on the LJ system is motivated by the simulation works of Kob *et al.*[16, 17, 20] in which the authors have considered a binary system in which masses for the two species are equal. We have therefore considered a fixed mass-ratio, $\Re = 1$ in investigating the LJ system. However, we believe that both the structure factors and the mass ratio have a role to play in deciding the transition point.

4. DISCUSSION

In the present work, we have used a recently proposed Mode-Coupling model for the glass transition in a two-component liquid to study the effect of mass-ratio of its constituent particles on the dynamic transition

predicted by the model equations. In the earlier mode coupling models[19] for the glass transition the dependence of the transition point on the mass-ratio of the two components is absent. This dependence of the dynamic transition on the ratio $\mathfrak{R}$ in the present model follows in a very natural way from the consideration of the proper set of equations of motion for the conserved variables. These equations are obtained following the same approach as was done for MCT in one component systems[3] or for the linearized dynamics of a two component system.[21] In the case of the binary mixtures, the motion of the smaller particles in the matrix of the bigger particles satisfy both conservation of mass and momentum which plays crucial role in freezing of the time scales of relaxation. For a mixture with fixed values of the relative abundance x and size ratio α, our result shows that no significant change in the transition density occurs for $\mathfrak{R} \geqslant 2$. A similar trend is also seen in the MD simulation of binary mixtures.[10, 11] However for the ratio $\mathfrak{R}$ smaller than unity, we find that transition point continuously shifts toward the higher densities. For a mixture of equally abundant species, if the bigger sized particles are lighter than the smaller particles, a considerable change in the dynamics occurs shifting the dynamic transition point to the higher densities.

The influence of the mass-ratio on the dynamical properties of a two-component liquid has already been observed earlier in computer simulation studies[22] and was subsequently analyzed in theoretical works on binary mixtures.[23, 24] However these studies were done for low densities and the mass of smaller particle was much smaller than that of the bigger one. In the present work we showed that the mass-ratio of particles of two different species will influence their relative motion and therefore will have an effect on the dynamic instability approaching high density. This ratio starts showing the influence when smaller sized particles have mass which is more than that of the bigger particles.

The physical significance of the observed mass ratio dependence can also be interpreted in the following manner: In case of a binary mixture with unequal masses for two species the process of jamming has to be considered with respect to the motion of one species (less abundant type) in the matrix of the other. We shall refer the species with lower mass and higher mass as "lighter" and "heavier," respectively. Let us consider the case where the bigger sized spheres are 80% and smaller ones are 20% in numbers. In such a situation, if the bigger sized particles are much lighter (i.e., $\mathfrak{R} \ll 1$) then they bounce off with higher speed in collisions with smaller sized particles and can easily swim through the matrix of the smaller (heavier) species thus allowing fluidity to be maintained till very high packing fraction. On the other hand if the big particles are much heavier ($\mathfrak{R} \gg 1$) the smaller sized particles (lighter) get trapped quite easily

in the sea of bigger particles. Thus for higher values of mass ratio the jamming occurs easily.

The situation however gets reversed if the bigger sized particles are only 20% and the smaller ones are 80%. In this case if the bigger sized particles are light ($\Re \ll 1$) they are unable to move through the sea of small (heavier) spheres and easily get trapped causing the jamming. If, on the other hand, the bigger particles are much heavier ($\Re \gg 1$) they can still push through the sea of smaller ones (lighter) and thus delay the jamming process. This physical argument can be made more clear from Fig. 7, where we have shown the variation in the transition point with $\Re$ for $x = 0.8$ (squares) and 0.2 (circles) at the same size-ratio, $\alpha = 0.8$. Here for the larger concentration (80%) of the smaller particles, at the same size-ratio, an opposite behavior is observed. Now the transition density is almost constant for low mass-ratio and shifts to higher values as $\Re$ is increased much beyond 1.

The MCT instability is a dynamic one occurring usually in the higher temperature range and causes a qualitative change in the dynamics (T_c). This is distinct from the models where a transition occurs due to an entropy crisis (T_g). Here (MCT) development of long relaxation times solely come from the dynamics of the fluid with structural input (initial condition). It should be noted that Eq. (12) in the present manuscript for the NEPs depends only upon the mass-ratio ($\Re$) of two species and *does not* depend on the individual masses of the two particles. The influence

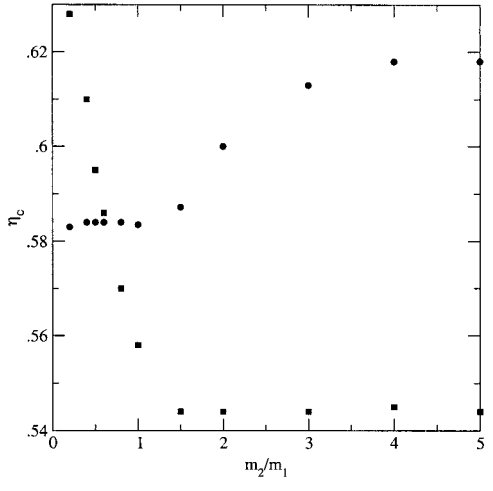

Fig. 7. Transition density, η_c, is plotted with $\Re$ for two different values of $x = 0.8$ (squares) and 0.2 (circles) at $\alpha = 0.8$.

of the ratio $\mathfrak{R}$ on the dynamics as seen here cannot be simply removed through a choice of variables as was recently proposed for a molecular liquid.[25] The ideal dynamic transition as defined by the nonzero values of the NEPs is not observable in a MD simulation. However it is always possible to make an estimation of the NEPs through the von Schweidler power law fit to the density correlation functions over the intermediate time scales. Therefore in a MD simulation, it is easier to test the theory predictions for the mass-ratio dependence of NEPs than the dynamic transition itself.

For the LJ system our model equations show that dynamic transition is absent till low temperature. Here one has to consider more closely how the "transition point" is obtained in the computer simulation works. In the simulation work of Kob *et al.*, a prediction for dynamic transition was made by fitting a power law form to the diffusion data at low temperatures. The extrapolated temperature where the diffusion coefficient appeared to go to zero was taken to be the transition point.

Finally, studying the mass-ratio ($\mathfrak{R}$) dependence of the transition point in LJ system requires calculation for the transition point at different temperatures. Therefore we need structure factors at all temperatures. The structure factor for the LJ system obtained through the solution of the integral equations is also not very reliable at low temperatures. In the present work we have therefore not done such an analysis for the LJ system. However we do not expect any qualitative change in the dependence of the transition point on the mass ratio $\mathfrak{R}$ in this case as compared to the hard spheres.

ACKNOWLEDGMENTS

U.H. acknowledges the financial support from the University Grant Commission, India.

REFERENCES

1. U. Bengtzelius, W. Gőtze, and A. Sjőlander, *J. Phys. C Solid State Phys.* **17**:5915–5934 (1984).
2. S. P. Das, G. F. Mazenko, S. Ramaswamy, and J. J. Toner, *Phys. Rev. Lett.* **54**:118 (1985).
3. S. P. Das and G. F. Mazenko, *Phys. Rev. A* **34**:2265 (1986).
4. W. Gotze, *Liquids, Freezing, and The Glass Transition*, J. P. Hansen, D. Levesque, and J. Zinn-Justin, eds. (Elsevier, New York, 1991).
5. B. Frick, B. Farago, and D. Richter, *Phys. Rev. Lett.* **64**:2921 (1990).
6. W. Gotze, *Z. Phys. B: Condens. Matter* **60**:195–203(1985).
7. J. L. Barrat, W. Gotze, and A. Latz, *J. Phys.: Condens. Matter* **1**:7163 (1989).

8. J. L. Barrat and A. Latz, *J. Phys.: Condens. Matter* **2**:4289–4295(1990).
9. U. Harbola and S. P. Das, *Phys. Rev. E* **65**:036138 (2002).
10. B. Bernu, J. P. Hansen, Y. Hiwatari, and G. Pastore, *Phys. Rev. A* **36**:4891 (1987).
11. J. N. Roux, J. L. Barrat, and J. P. Hansen, *J. Phys.: Condens. Matter* **1**:7171 (1989); J. L. Barrat, M. Baus, and J. P. Hansen, *J. Phys. C* **20**:1413 (1987).
12. S. K. Ma and G. F. Mazenko, *Phys. Rev. B* **11**:4077 (1975).
13. S. Sinha and M. C. Marchetti, *Phys. Rev. A* **46**:4942 (1992).
14. N. W. Ashcroft and D. C. Langreth, *Phys. Rev.* **156**:685 (1967).
15. J. L. Lebowitz, *Phys. Rev. A* **133**:895 (1964).
16. W. Kob and H. C. Andersen, *Phys. Rev. E* **51**:4262 (1995); *Phys. Rev. Lett.* **73**:1376 (1994).
17. W. Kob and H. C. Andersen, *Phys. Rev. Lett.* **73**:1376 (1994).
18. D. M. Due and D. Henderson, *J. Chem. Phys.* **104**:6742 (1996).
19. J. S. Thakur and J. Bosse, *Phys. Rev. A* **43**:4378 (1991); *Phys. Rev. A* **43**:4388 (1991); J. L. Barrat and A. Latz, *J. Phys.: Condens. Matter* **2**:4389 (1990).
20. M. Nauroth and W. Kob, *Phys. Rev. E* **55**:657 (1996).
21. C. Cohen, J. W. H. Sutherland, and J. M. Deutch, *Phys. Chem. Liquids* **2**:213–235 (1971).
22. A. Rahman and F. H. Stillinger, *Phys. Rev. A* **10**:368 (1974).
23. J. Bosse and W. Schirmacher, *Phys. Rev. Lett.* **57**:3277 (1986).
24. A. Campa and E. G. D. Cohen, *Phys. Rev. Lett.* **61**:853 (1988); *Phys. Rev. A* **39**:4909 (1989); **41**:5451 (1990).
25. R. Schilling, *Phys. Rev. E* **65**:051206 (2002).